Study on Obtaining Convex Shape of Solid-Liquid Interface under Microgravity

Satoshi Adachi †, Katsumi Takahashi ††, Keiichi Kuwahara †††, Hirokazu Kato ††††, and Kyoichi Kinoshita ††††

† Fundamental Technology Dept, Research Institute, Ishikawajima-Harima Heavy Industries Co., Ltd., 1-15, Toyosu 3-chome, Koto-ku, Tokyo 135-8732 Japan

† † Environmental Process Development Dept., Research Institute, Ishikawajima-Harima Heavy Industries Co., Ltd., 1, Shin-Nakahara-cho, Isogo-ku, Yokohama-shi, Kanagawa 235-8501 Japan

† † † Space Experiment System Development Department, Space Development Division, Aero-Engine & Space Operations, Shin-Otemachi Bldg., 2-1, Otemachi 2-chome, Chiyoda-ku, Tokyo 100-8182 Japan

† † † † Space Utilization Research Center, Office of Space Utilization Systems, National Space Development Agency of Japan, 1-1, Sengen 2-chome, Tsukuba-shi, Ibaraki 305-8505 Japan

In order to investigate condition to grow semiconductor crystal with a convex solid-liquid interface under microgravity, numerical calculation is carried out. In this study, the boundary fitted coordinate (BFC) method is used. The thermal conduction equation in the cylindrical coordinates is used as the governing equation. To get the better numerical stability, several transformation techniques are considered. To evaluate the reliability of the numerical result, the calculation result is compared with the experimental one.

1. Introduction

In a melt growth technique using a crucible such as the Bridgeman method, a shape of a solid-liquid interface should be convex toward melt in order to grow a single crystal. This is because it is expected that polycrystallization can be reduced by the convex shape. Generally, an interface and a grain boundary macroscopically grow perpendicularly to the interface. Therefore, a nuclear appearing around the crucible wall will impacts with the wall, and will be extinguished before developing into a grain boundary if an interface shape is convex.

On the earth, it is achieved that an interface becomes convex by optimizing a furnace for the specific material, including the furnace modification. However, in the microgravity experiments, it is difficult to optimize a furnace for a specific material due to a multipurpose furnace. Furthermore, limitations such as safety, power resource, weight and size make this optimization more difficult. Therefore, an interface shape is concave [1, 2] in the past melt growth experiment under the microgravity. Since only polycrystals or small single crystals can be obtained due to the concavity, the effectiveness of the microgravity experiments begins to be doubted.

In order to clear away such a doubt, it is required that a large single crystal enough to evaluate the characteristics should be obtained in the microgravity experiment. For this purpose, it is one of the extreme priority subjects to make the interface shape convex under the microgravity. However, the timely and various improvement of the furnace for the microgravity experiment similar to that on the earth is difficult as mentioned above. Then, it is required improving the performance of the ampoule and the cartridge to compensate the furnace performance [2, 3].

In this study, numerical analyses on the ampoule and the cartridge were carried out in order to obtain the convex shape that is not achieved in the microgravity experiment until now. These analyses are not only useful for the microgravity experiment but also useful for the ground experiment such as the vertical Bridgeman method,

which is the similar configuration to the microgravity experiment. Namely, there is the possibility that the results of the research related to the microgravity experiment can be applied to the research on the earth. This is one of the most important points of view in the present microgravity experiment.

In this paper, the numerical model is described in the next section, the numerical results in §3, discussion in §4, and finally summarized.

2. Numerical Model

In this study, in order to obtain the solid-liquid interface shape, the boundary fitted coordinate (BFC) method [4-7] which is a kind of the difference method is used. The BFC method solves the governing equation on the virtual rectangular space by using the coordinates in the actual space where is mapped onto the virtual space.

Generally, when a discrete equation is solved numerically, it is required satisfying a following condition;

(1) a boundary shape can be handled accurately,

(2) a node can be configured densely to the area where a physical parameter varies greatly, and,

(3) a node can be configured smoothly in the whole calculation area.

If the above condition can not be satisfied, the accuracy of the solution, the stability, the convergence and so on will be deteriorated. The finite element method (FEM) can satisfy the condition (1) easily. However, many experiences and the amount of activity are often required so that the FEM may satisfy the condition (2) and (3). The BFC method can also generate a node along the boundary automatically due to the inverse mapping from the virtual space to the actual space. Therefore, the BFC method is applied in this study.

In this paper, the interface shape is determined by only the temperature, that is, the material is assumed to be the element or the binary compound. In addition, since the gravity under the microgravity is less than or equals to 10^{-4} as compared with that on the earth, the amount by the thermal transport by the thermal convection is neglected. Namely, in order to obtain the temperature distribution, only the thermal conduction equation in the steady state is solved. The steady state means that the heat flux by the latent heat is assumed relatively small. This is true when the solidification progresses slowly like the semiconductor crystal growth. Thus, the governing equation is represented as follows;

$$\frac{\partial^2 T}{\partial r^2}+\frac{1}{r}\frac{\partial T}{\partial r}+\frac{\partial^2 T}{\partial z^2}=0 \quad , (1)$$

where, T is the temperature, r and z are the cylindrical coordinates in the physical space, respectively.

Here, the coordinates of r and z in eq. (1) are transformed to the coordinates of ξ and η in the virtual rectangular space. The coordinates r and z can be represented by using the coordinates ξ and η, that is,

$$\begin{pmatrix} dr \\ dz \end{pmatrix}=\begin{pmatrix} r_\xi & r_\eta \\ z_\xi & z_\eta \end{pmatrix}\begin{pmatrix} d\xi \\ d\eta \end{pmatrix} \quad , (2)$$

where, the subscriptions represent the partial differentiation. Equation (2) is rewritten by multiplying the inverse matrix as

$$\begin{pmatrix} d\xi \\ d\eta \end{pmatrix}=\frac{1}{J}\begin{pmatrix} z_\eta & -r_\eta \\ -z_\xi & r_\xi \end{pmatrix}\begin{pmatrix} dr \\ dz \end{pmatrix} \quad , (3)$$

where, J is Jacobian, $r_\xi z_\eta - r_\eta z_\xi$.

Another expression of ξ and η can be written as

$$\begin{pmatrix} d\xi \\ d\eta \end{pmatrix}=\begin{pmatrix} \xi_r & \xi_z \\ \eta_r & \eta_z \end{pmatrix}\begin{pmatrix} dr \\ dz \end{pmatrix} \quad . (4)$$

By comparison between eq. (3) and eq. (4), the expressions partially differentiated of ξ and η can be obtained;

$$\xi_r=\frac{z_\eta}{J}, \quad \xi_z=-\frac{r_\eta}{J}, \quad \eta_r=-\frac{z_\xi}{J}, \quad \eta_z=\frac{r_\xi}{J} \quad . (5)$$

Thus, eq. (1) can be transformed by using eq. (5) as described in the appendix A;

$$\alpha T_{\xi\xi}-2\beta T_{\xi\eta}+\gamma T_{\eta\eta}+\frac{2}{r}J\left(T_\xi z_\eta - T_\eta z_\xi\right)=0 \quad , (6)$$

where, $\alpha = r_\eta^2 + z_\eta^2$, $\beta = r_\xi r_\eta + z_\xi z_\eta$, $\gamma = r_\xi^2 + z_\xi^2$. By solving this equation, the temperature in the virtual space can be obtained.

The heat flux must be equal at both side of the boundary, that is,

$$-\kappa \left| \frac{\partial T}{\partial n} \right| = const. \quad (7)$$

By transforming this equation, two expressions are obtained;

$$\frac{\kappa}{J\sqrt{\gamma}} \left(\beta T_\xi - \gamma T_\eta \right) = const. \text{ , and, } (8)$$

$$\frac{\kappa}{J\sqrt{\alpha}} \left(\alpha T_\xi - \beta T_\eta \right) = const. \quad (9)$$

The first equation is perpendicular direction to the function $\eta = const.$, and the other one is to the function $\xi = const.$.

In order to convert the temperature in the virtual space to that in the real space, the relationship between the virtual and the real coordinates is required. In this paper, the relationship based on the Laplace equation is used, that is,

$$\frac{\partial^2 \xi}{\partial r^2} + \frac{1}{r}\frac{\partial \xi}{\partial r} + \frac{\partial^2 \xi}{\partial z^2} = 0 \text{ , and, } (10)$$

$$\frac{\partial^2 \eta}{\partial r^2} + \frac{1}{r}\frac{\partial \eta}{\partial r} + \frac{\partial^2 \eta}{\partial z^2} = 0 \quad (11)$$

The nodes generated by the Laplace equation are well known to be suitable for the BFC method [4-6]. Equations (10) and (11) can be transformed as described in Appendix B;

$$\alpha r_{\xi\xi} - 2\beta r_{\xi\eta} + \gamma r_{\eta\eta} + \frac{1}{r} J^2 = 0 \text{ , and, } (12)$$

$$\alpha z_{\xi\xi} - 2\beta z_{\xi\eta} + \gamma z_{\eta\eta} = 0 \quad (13)$$

These equations are applied for the ampoule shown in Fig. 1. The ampoule is based on the ampoule used in the past Japanese experiment under microgravity [2, 3], however, it is more improved in order to obtain the convex interface shape. In the past microgravity experiment, the highest temperature side is adiabatic due to vacuum, and the lowest temperature side is near adiabatic in order to save the power. Therefore, the heat flows from the ampoule surface at the highest temperature to the surface at the lowest temperature. Since the interface shape is perpendicular to the heat flux in principle, if the container seal is near the sample, the shape becomes concave. In order to prevent the concave shape, it is required that the heat flows along the axis. The heat sink installed adjacently to the sample would modify the flow.

Since the ampoule is usually set in the cartridge as shown in Fig. 2, the whole cartridge is modeled.

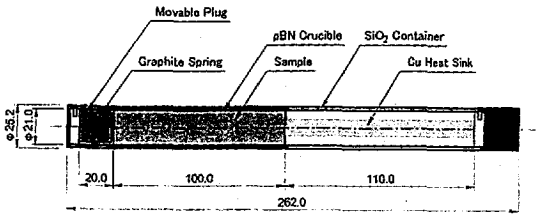

Fig. 1 Schematic View of Ampoule

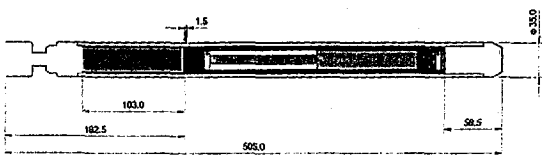

Fig. 2 Schematic View of Cartridge

Fig. 3 Generated Grid

One example of the generated grid by using eqs. (12) and (13) is shown in Fig. 3. By using such a grid, the temperature distribution is calculated.

3. Calculation Results

In this section, the interface shape is investigated from the calculation results of the temperature distribution by using the generated grid. To calculate the distribution, the thermal conductivity of the solid sample is assumed to be 1.2 W/m·K and the melt is to be 2.5 times as

large as the solid. The boundary condition at the end of the highest temperature side is adiabatic, and that at the opposite end is constant temperature. On the cartridge surface is given the fixed temperature profile. Although the actual temperature profile of the furnace can be expressed as a polynomial function, this profile makes the shape variety complicated. Hence, in order to understand more easily the shape behavior, the temperature profile is approximated to simpler one.

The interface usually exists at the point of inflexion. This means that the temperature gradient is low in the region where the temperature is higher than that at the interface, and the gradient is high in the region where the temperature is lower than that at the interface. Namely, the two kinds of the temperature characteristics are used for the crystal growth. Therefore, the combination of the two linear profiles is used in this analysis. The used temperature gradients are 20 K/cm and 80 K/cm. The temperature is clipped at the highest temperature of 1527 K and the lowest one of 317 K to prevent giving unrealistic profile.

The obtained typical result is shown in Fig. 4. The interface location on the axis is about 174.3 mm, where 13.2 mm far from the lowest end of the sample. At this location, the interface shape is convex as shown in Fig. 5. The convex length, which is defined as the difference between the locations on the axis and on the crucible inner wall, is about 3 mm. Since this length should decrease with increasing the distance from the heat sink, the dependency of the convex length on the interface location is investigated and is shown in Fig. 6. This figure shows that the interface is convex in about 80 % of the total sample length. This is valuable result for the microgravity experiment, but this result seems that the effect of the heat sink is different at the interface location. The reason should be due to the temperature profile, that is, the saturated temperature profile in the lower temperature region makes the heat flux towards the lower temperature side decrease. To improve this, the temperature gradient must keep steep, however, it might be essentially impossible because the present lowest temperature is set near the room temperature.

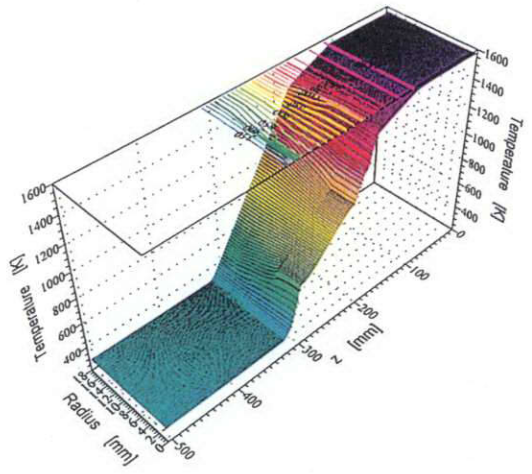

Fig.4 Typical Result of Temperature Distribution Calculation

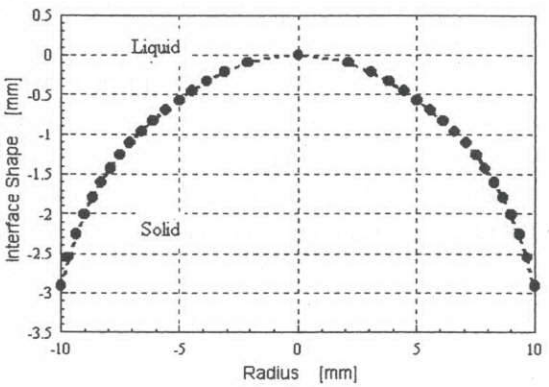

Fig.5 Interface Shape

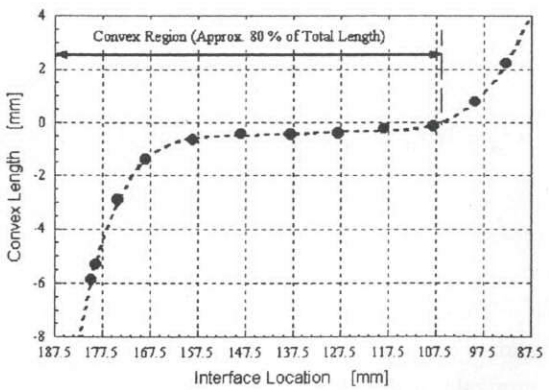

Fig.6 Dependency of Convex Length on Interface Location

4.Discussion

In order to evaluate the reliability of the numerical analysis, the calculation result is compared with the experimental one obtained on the earth. In this experiment, the ampoule shown in Fig. 3 is used. The temperature profile and the ampoule location are shown in Fig. 7. The right side in this figure is actually top and the left side bottom. Therefore, the influence of the thermal convection should be small.

The temperature gradient is set as large as possible, however, it is not large enough to make the interface convex because of using the isothermal furnace. To solidify the sample, the gradient freezing method is used. In the experiment, the sample is InSb, the binary compound semiconductor, since the interface location and shape are determined only by the temperature. This is suitable for the present numerical analysis solving the steady state thermal conduction equation.

The external view of the InSb sample is shown in Fig. 8. In Fig. 8, several lines can be observed. The first one, that is the most left one, is the initial interface, and the others are the marking generated by holding the temperature for about 30 minutes. The longitudinal cross section is shown in Fig. 9. The marking can be observed on the sample surface, however, except for the initial interface, it cannot be observed on the cut plain, that is, the inside of the sample. Therefore, the initial interface shape is compared with the numerically obtained shape. The comparison is shown in Fig. 10. From Fig. 10, it is clarified that the numerical results well agree with the experimental ones. This represents the reliability of this analysis.

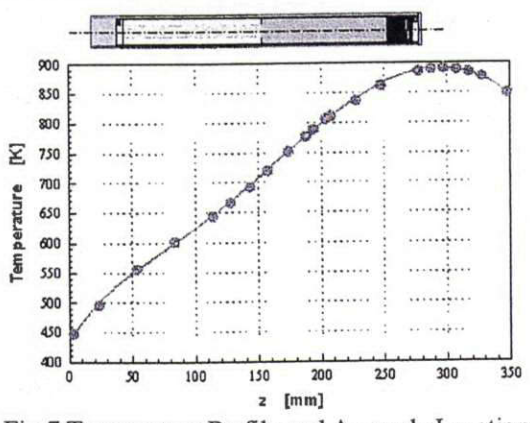

Fig.7 Temperature Profile and Ampoule Location

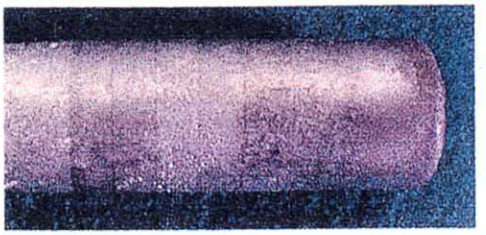

Fig.8 External View of InSb Sample

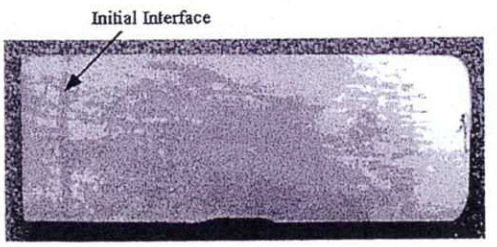

Fig.9 Longitudinal Cross Section of InSb Sample

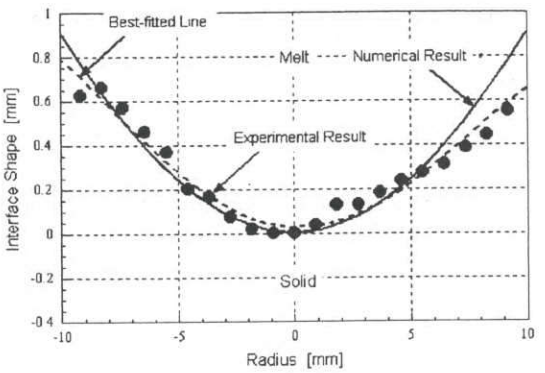

Fig.10 Comparison of Numerical Result with Experimental One

5. Conclusions

The method of the coordinates transformation in the cylindrical coordinates is established. By using this method, the ampoule and the cartridge are modeled. The grid can be generated and be obtained numerical solutions. From the numerical results, it is clarified that the initial interface shape is convex and the convex shape can be kept in about 80 % of the total sample length. Although the effect of the heat sink is decreases with increasing the distance from the sample end at the lower temperature side, about 0.4 mm of the convex length can be kept.

In order to investigate the reliability of the

numerical results, these results are compared with the experimental results. It is clarified that the numerical results well agree with the experimental ones. This represents the reliability of the numerical calculation.

Acknowledgement

To carry out this study, both the fund of the National Space Development Agency of Japan (NASDA) and the in-house budget are introduced. The authors are thankful to Prof. Maekawa at Toyo Univ. for his valuable advice and discussion.

References

1) J. M. Bly, M. L. Kaforey, D. H. Matthiesen and A. Chait: *Proc. of the 1996 10th American Conf. on Cryst. Growth and the 9th Int. Conf. on Vapor Growth and Epitaxy, Vail, 1996,* J. Cryst. Growth, 174 (1997) Suppl. 1-4, pp. 220-225.

2) S. Adachi, M. Miyuki, K. Takahashi and H. Sakai: *Proc. of Symp. on SFU Experiments for Industries, Tokyo, 1996* (Institute for Unmanned Space Experiment Free Flyer, 1996).

3) S. Adachi, K. Takahashi and Y Ikegami: Abstr. (123rd TMS Annual Meet. and Exhibition 1994); The Mineral, Metals & Materials Society, p.22.

4) J. F. Thompson, F. C. Thames and C. W. Mastin: J. Comp. Phys. 15 (1974) 299.

5) K. Fujii: *Numerical Methods for Computational Fluid Dynamics* (Tokyo Univ., Tokyo, 1994) 2nd ed., Chap. 7 [in Japanese].

6) H. Takami and T. Kawamura: *Numerical Solution of Partial Differential Equations by the Finite Difference Method* (Tokyo Univ., Tokyo, 1994) 2nd ed., Chap. 6 [in Japanese].

7) M. Saitou: Inst. Electron. Mater. Tech. Note 7 (1989) No. 2, 15 [in Japanese].

Appendix A

Thermal conduction equation in steady state can be written as

$$\frac{\partial^2 T}{\partial r^2}+\frac{1}{r}\frac{\partial T}{\partial r}+\frac{\partial^2 T}{\partial z^2}=0\ . \tag{A-1}$$

Each term is transformed by using virtual rectangular coordinates ξ and η;

$$\frac{\partial T}{\partial r}=\frac{\partial T}{\partial \xi}\frac{\partial \xi}{\partial r}+\frac{\partial T}{\partial \eta}\frac{\partial \eta}{\partial r}=T_\xi \xi_r+T_\eta \eta_r\ , \tag{A-2}$$

$$\begin{aligned}
\frac{\partial^2 T}{\partial r^2}&=\frac{\partial}{\partial r}\left(\frac{\partial T}{\partial \xi}\frac{\partial \xi}{\partial r}+\frac{\partial T}{\partial \eta}\frac{\partial \eta}{\partial r}\right)\\
&=\frac{\partial \xi}{\partial r}\frac{\partial}{\partial r}\left(\frac{\partial T}{\partial \xi}\right)+\frac{\partial T}{\partial \xi}\frac{\partial}{\partial r}\left(\frac{\partial \xi}{\partial r}\right)+\frac{\partial \eta}{\partial r}\frac{\partial}{\partial r}\left(\frac{\partial T}{\partial \eta}\right)+\frac{\partial T}{\partial \eta}\frac{\partial}{\partial r}\left(\frac{\partial \eta}{\partial r}\right)\\
&=\frac{\partial \xi}{\partial r}\left(\frac{\partial \xi}{\partial r}\frac{\partial}{\partial \xi}+\frac{\partial \eta}{\partial r}\frac{\partial}{\partial \eta}\right)\left(\frac{\partial T}{\partial \xi}\right)+\frac{\partial T}{\partial \xi}\frac{\partial^2 \xi}{\partial r^2}\\
&\quad+\frac{\partial \eta}{\partial r}\left(\frac{\partial \xi}{\partial r}\frac{\partial}{\partial \xi}+\frac{\partial \eta}{\partial r}\frac{\partial}{\partial \eta}\right)\left(\frac{\partial T}{\partial \eta}\right)+\frac{\partial T}{\partial \eta}\frac{\partial^2 \eta}{\partial r^2}\\
&=\xi_r{}^2 T_{\xi\xi}+\xi_r\eta_r T_{\xi\eta}+T_\xi \xi_{rr}+\xi_r\eta_r T_{\xi\eta}+\eta_r{}^2 T_{\eta\eta}+T_\eta \eta_{rr}\\
&=\xi_r{}^2 T_{\xi\xi}+2\xi_r\eta_r T_{\xi\eta}+\eta_r{}^2 T_{\eta\eta}+T_\xi \xi_{rr}+T_\eta \eta_{rr}
\end{aligned}\ , \tag{A-3}$$

$$\frac{\partial^2 T}{\partial z^2}=\xi_z{}^2 T_{\xi\xi}+2\xi_z\eta_z T_{\xi\eta}+\eta_z{}^2 T_{\eta\eta}+T_\xi \xi_{zz}+T_\eta \eta_{zz}\ . \tag{A-4}$$

Equations (A-2) - (A-4) are substituted to eq. (A-1), that is,

$$\begin{aligned}
&\frac{\partial^2 T}{\partial r^2}+\frac{1}{r}\frac{\partial T}{\partial r}+\frac{\partial^2 T}{\partial z^2}\\
&=\xi_r{}^2 T_{\xi\xi}+2\xi_r\eta_r T_{\xi\eta}+\eta_r{}^2 T_{\eta\eta}+T_\xi\xi_{rr}+T_\eta\eta_{rr}+\frac{1}{r}\left(T_\xi\xi_r+T_\eta\eta_r\right)\\
&+\xi_z{}^2 T_{\xi\xi}+2\xi_z\eta_z T_{\xi\eta}+\eta_z{}^2 T_{\eta\eta}+T_\xi\xi_{zz}+T_\eta\eta_{zz}\\
&=\left(\xi_r{}^2+\xi_z{}^2\right)T_{\xi\xi}+2\left(\xi_r\eta_r+\xi_z\eta_z\right)T_{\xi\eta}+\left(\eta_r{}^2+\eta_z{}^2\right)T_{\eta\eta}\\
&+\left(\xi_{rr}+\xi_{zz}\right)T_\xi+\left(\eta_{rr}+\eta_{zz}\right)T_\eta+\frac{1}{r}\left(T_\xi\xi_r+T_\eta\eta_r\right)
\end{aligned} \tag{A-5}$$

Here, the relationships between real and virtual space are described as shown in Appendix B;

$$\xi_{rr}+\xi_{zz}=\frac{1}{r}\xi_r, \text{ and} \tag{A-6}$$

$$\eta_{rr}+\eta_{zz}=\frac{1}{r}\eta_r\ . \tag{A-7}$$

Therefore, eq. (A-5) can be rewritten as

$$\begin{aligned}
&\frac{\partial^2 T}{\partial r^2}+\frac{1}{r}\frac{\partial T}{\partial r}+\frac{\partial^2 T}{\partial z^2}\\
&=\left(\xi_r{}^2+\xi_z{}^2\right)T_{\xi\xi}+2\left(\xi_r\eta_r+\xi_z\eta_z\right)T_{\xi\eta}+\left(\eta_r{}^2+\eta_z{}^2\right)T_{\eta\eta}\\
&\qquad+\frac{1}{r}T_\xi\xi_r+\frac{1}{r}T_\eta\eta_r+\frac{1}{r}\left(T_\xi\xi_r+T_\eta\eta_r\right)\\
&=\left(\xi_r{}^2+\xi_z{}^2\right)T_{\xi\xi}+2\left(\xi_r\eta_r+\xi_z\eta_z\right)T_{\xi\eta}+\left(\eta_r{}^2+\eta_z{}^2\right)T_{\eta\eta}\\
&\qquad+\frac{2}{r}\left(T_\xi\xi_r+T_\eta\eta_r\right)\\
&=\frac{1}{J^2}\left\{\alpha T_{\xi\xi}-2\beta T_{\xi\eta}+\gamma T_{\eta\eta}+\frac{2}{r}J\left(T_\xi z_\eta-T_\eta z_\xi\right)\right\}=0
\end{aligned} \tag{A-8}$$

where, $\alpha=r_\eta^2+z_\eta^2$, $\beta=r_\xi r_\eta+z_\xi z_\eta$, $\gamma=r_\xi^2+z_\xi^2$. Equation (A-8) is solved to obtain the temperature distribution in this study.

It should be noted that the different expression of the thermal conduction equation is obtained by using the different relationships instead of eqs. (A-6) and (A-7). For example, when the Laplace equations of eqs. (A-10) and (A-11) are substituted into eq. (A-5), the term of $1/r$ in eq. (A-8) can be eliminated, that is,

$$\begin{aligned}
&\frac{\partial^2 T}{\partial r^2}+\frac{1}{r}\frac{\partial T}{\partial r}+\frac{\partial^2 T}{\partial z^2}\\
&=\frac{1}{J^2}\left(\alpha T_{\xi\xi}-2\beta T_{\xi\eta}+\gamma T_{\eta\eta}\right)=0
\end{aligned} \tag{A-9}$$

$$\xi_{rr}+\frac{1}{r}\xi_r+\xi_{zz}=0 \tag{A-10}$$

$$\eta_{rr}+\frac{1}{r}\eta_r+\eta_{zz}=0 \tag{A-11}$$

Equation (A-9) is the same expression of the thermal conduction equation in the case of the rectangular real space. This equation is simple as compared with eq. (A-8) and can be easily solved, however, it is difficult to solve eqs. (A-10) and (A-11) due to the effect of the term of $1/r$ as described in Appendix B. These equations indicate that the cylindrical coordinates in the real space is transformed to the rectangular coordinates in the virtual space by eqs. (A-10) and (A-11).

Appendix B

It is well known that the good relationships between the real and the virtual rectangular coordinates are described as the Laplace equation;

$$\xi_{rr} + \frac{1}{r}\xi_r + \xi_{zz} = 0, \text{ and} \tag{B-1}$$

$$\eta_{rr} + \frac{1}{r}\eta_r + \eta_{zz} = 0 \tag{B-2}$$

These equations are transformed by using the partial differentiation of r, z by ξ, η. Each term in eq. (B-1) can be represented as

$$\xi_r = \frac{z_\eta}{J}, \tag{B-3}$$

$$\begin{aligned}\xi_{rr} &= \frac{\partial}{\partial r}\left(\frac{z_\eta}{J}\right) = \left(\xi_r \frac{\partial}{\partial \xi} + \eta_r \frac{\partial}{\partial \eta}\right)\left(\frac{z_\eta}{J}\right) \\ &= \xi_r \frac{\frac{\partial z_\eta}{\partial \xi}J - \frac{\partial J}{\partial \xi}z_\eta}{J^2} + \eta_r \frac{\frac{\partial z_\eta}{\partial \eta}J - \frac{\partial J}{\partial \eta}z_\eta}{J^2}\end{aligned}, \text{ and,} \tag{B-4}$$

$$\xi_{zz} = -\xi_z \frac{\frac{\partial r_\eta}{\partial \xi}J - \frac{\partial J}{\partial \xi}r_\eta}{J^2} - \eta_z \frac{\frac{\partial r_\eta}{\partial \eta}J - \frac{\partial J}{\partial \eta}r_\eta}{J^2}. \tag{B-5}$$

Now,

$$\frac{\partial J}{\partial \xi} = \frac{\partial}{\partial \xi}\left(r_\xi z_\eta - r_\eta z_\xi\right) = r_{\xi\xi} z_\eta + r_\xi z_{\xi\eta} - r_{\xi\eta} z_\xi - r_\eta z_{\xi\xi}, \text{ and,} \tag{B-6}$$

$$\frac{\partial J}{\partial \eta} = r_{\xi\eta} z_\eta + r_\xi z_{\eta\eta} - r_{\eta\eta} z_\xi - r_\eta z_{\xi\eta} \tag{B-7}$$

are substituted to eqs. (B-4) and (B-5);

$$\begin{aligned}\xi_{rr} &= \frac{1}{J^3}\left(r_\xi z_\eta^{\,2} z_{\xi\eta} - r_\eta z_\xi z_\eta z_{\xi\eta} - z_\eta^{\,3} r_{\xi\xi} - r_\xi z_\eta^{\,2} z_{\xi\eta}\right.\\ &\qquad + z_\xi z_\eta^{\,2} r_{\xi\eta} + r_\eta z_\eta^{\,2} z_{\xi\xi} - r_\xi z_\xi z_\eta z_{\eta\eta} + r_\eta z_\xi^{\,2} z_{\eta\eta}\\ &\qquad \left. + z_\xi z_\eta^{\,2} r_{\xi\eta} + r_\xi z_\xi z_\eta z_{\eta\eta} - z_\xi^{\,2} z_\eta r_{\eta\eta} - r_\eta z_\xi z_\eta z_{\xi\eta}\right),\\ &= \frac{1}{J^3}\left\{-z_\eta\left(z_\eta^{\,2} r_{\xi\xi} - 2z_\xi z_\eta r_{\xi\eta} + z_\xi^{\,2} r_{\eta\eta}\right)\right.\\ &\qquad \left. + r_\eta\left(z_\eta^{\,2} z_{\xi\xi} - 2z_\xi z_\eta z_{\xi\eta} + z_\xi^{\,2} z_{\eta\eta}\right)\right\}\end{aligned} \tag{B-8}$$

and,

$$\begin{aligned}\xi_{zz} &= \frac{1}{J^3}\left\{-z_\eta\left(r_\eta^{\,2} r_{\xi\xi} - 2r_\xi r_\eta r_{\xi\eta} + r_\xi^{\,2} r_{\eta\eta}\right)\right.\\ &\qquad \left. + r_\eta\left(r_\eta^{\,2} z_{\xi\xi} - 2r_\xi r_\eta z_{\xi\eta} + r_\xi^{\,2} z_{\eta\eta}\right)\right\}\end{aligned} \tag{B-9}$$

Finally, the transformation of eq. (B-1) is obtained as,

$$\begin{aligned}&\xi_{rr} + \frac{1}{r}\xi_r + \xi_{zz}\\ &= \frac{1}{J^3}\left\{-z_\eta\left(\alpha r_{\xi\xi} - 2\beta r_{\xi\eta} + \gamma r_{\eta\eta} - \frac{J^2}{r}\right) + r_\eta\left(\alpha z_{\xi\xi} - 2\beta z_{\xi\eta} + \gamma z_{\eta\eta}\right)\right\}\\ &= 0\end{aligned} \tag{B-10}$$

Equation (B-2) can also be transformed by using the similar way in the case of eq. (B-1),

$$\begin{aligned}&\eta_{rr} + \frac{1}{r}\eta_r + \eta_{zz}\\ &= \frac{1}{J^3}\left\{z_\xi\left(\alpha r_{\xi\xi} - 2\beta r_{\xi\eta} + \gamma r_{\eta\eta} - \frac{J^2}{r}\right) - r_\xi\left(\alpha z_{\xi\xi} - 2\beta z_{\xi\eta} + \gamma z_{\eta\eta}\right)\right\}\\ &= 0\end{aligned} \tag{B-11}$$

From eqs (B-10) and (B-11), the relationships between the real and the virtual coordinates can be rewritten as,

$$\alpha r_{\xi\xi} - 2\beta r_{\xi\eta} + \gamma r_{\eta\eta} - \frac{J^2}{r} = 0 \text{ , and,} \tag{B-12}$$

$$\alpha z_{\xi\xi} - 2\beta z_{\xi\eta} + \gamma z_{\eta\eta} = 0 \text{ .} \tag{B-13}$$

These equations are mathematically correct, however, it is technically difficult to solve the difference equations based on eq. (B-12). The difference equation is represented as,

$$\begin{aligned}&\alpha\left(r_{i+1,j} - 2r_{i,j} + r_{i-1,j}\right) - \beta\frac{r_{i+1,j+1} - r_{i+1,j-1} - r_{i-1,j+1} + r_{i-1,j-1}}{2}\\ &\qquad + \gamma\left(r_{i,j+1} - 2r_{i,j} + r_{i,j-1}\right) - \frac{J^2}{r_{i,j}} = 0\end{aligned} \tag{B-14}$$

Equation (B-14) is the 2nd order polynomial equation of $r_{i,j}$, and the solutions can be obtained as,

$$r_{i,j} = \frac{-B \pm \sqrt{B^2 - 4AC}}{2A}, \tag{B-15}$$

where,

$$A = 4(\alpha + \gamma), \tag{B-16}$$

$$B = -2\alpha\left(r_{i+1,j} + r_{i-1,j}\right) + \beta\left(r_{i+1,j+1} - r_{i+1,j-1} - r_{i-1,j+1} + r_{i-1,j-1}\right) - 2\gamma\left(r_{i,j+1} + r_{i,j-1}\right), \text{ and,} \tag{B-17}$$

$$C = J^2 . \tag{B-18}$$

Equation (B-15) shows that $\left(B^2 - 4AC\right)$ may be less than 0. And $r_{i,j}$ may have 2 solutions, however, one pair of r and z must correspond to one pair of ξ and η. Hence, eq. (B-12) must be expressed by using another relationship so that only one $r_{i,j}$ can be obtained. These problems indicate that the transformation of the cylindrical coordinates to the rectangular coordinates is difficult near the axis. Since the cell volume near the axis is small as compared with one far from the axis, the mapped cell volume near the boundary corresponding to the axis must be small. This causes that the node density near the axis becomes high. This should be the reason of the transformation difficulty.

Now, instead of the Laplace equation firstly used, the Poisson equation is considered, that is,

$$\xi_{rr} + \frac{1}{r}\xi_r + \xi_{zz} = P, \text{ and} \tag{B-19}$$

$$\eta_{rr} + \frac{1}{r}\eta_r + \eta_{zz} = Q . \tag{B-20}$$

These equations are transformed by the same way of the case of eqs. (B-1) and (B-2);

$$\alpha r_{\xi\xi} - 2\beta r_{\xi\eta} + \gamma r_{\eta\eta} - \frac{J^2}{r} = -J^2\left(P r_\xi + Q r_\eta\right), \text{ and,} \tag{B-21}$$

$$\alpha z_{\xi\xi} - 2\beta z_{\xi\eta} + \gamma z_{\eta\eta} = -J^2\left(P z_\xi + Q z_\eta\right). \tag{B-22}$$

Although the method how the functions P and Q determine is well studied, that is so complicated. In this case, the fundamental problem is the effect of $1/r$. Therefore, it is enough to determine P and Q so that the term of $1/r$ can be eliminated. After here, the two cases are considered.

(1) Case of $Pr_\xi + Qr_\eta = \frac{1}{r}$ and $Pz_\xi + Qz_\eta = 0$

In this case, eqs. (B-19) – (B-22) are11 rewritten as

$$\xi_{rr} + \xi_{zz} = 0 , \tag{B-23}$$

$$\eta_{rr} + \eta_{zz} = 0 , \tag{B-24}$$

$$\alpha r_{\xi\xi} - 2\beta r_{\xi\eta} + \gamma r_{\eta\eta} = 0 \text{ , and,} \tag{B-25}$$

$$\alpha z_{\xi\xi} - 2\beta z_{\xi\eta} + \gamma z_{\eta\eta} = 0 \text{ .} \tag{B-26}$$

These equations are usually used in the case of the rectangular real space. This means that the coordinates system in the real space is simply mapped to the same system in the virtual space. While eqs. (B-25) and (B-26) can be simultaneously solved, the obtained grid are not so good for the analyses of the ampoule and the cartridge. Thus the second case is considered.

(2) Case of $Pr_{\xi} + Qr_{\eta} = \frac{2}{r}$ and $Pz_{\xi} + Qz_{\eta} = 0$

In this case, eqs. (B-19) – (B-22) are rewritten as

$$\xi_{rr} + \xi_{zz} = -\frac{1}{r}\xi_{r} \text{ ,} \tag{B-27}$$

$$\eta_{rr} + \eta_{zz} = -\frac{1}{r}\eta_{r} \text{ ,} \tag{B-28}$$

$$\alpha r_{\xi\xi} - 2\beta r_{\xi\eta} + \gamma r_{\eta\eta} + \frac{J^2}{r} = 0 \text{ , and,} \tag{B-29}$$

$$\alpha z_{\xi\xi} - 2\beta z_{\xi\eta} + \gamma z_{\eta\eta} = 0 \text{ .} \tag{B-30}$$

These equations can be also solved. The solutions are better than those in the previous case. Therefore, these relationships between the real and virtual space are used in this paper.